Chemical Physics Impact 8 (2024) 100481

Contents lists available at ScienceDirect

Chemical Physics Impact

journal homepage: www.sciencedirect.com/journal/chemical-physics-impact

Full Length Article

Solvation effects, structural, vibrational analysis, chemical reactivity, nanocages, ELF, LOL, docking and MD simulation on Sitagliptin

G. Venkatesh [a,*], S. Haseena [b], P. Vennila [c], Yudibeth Sixto-López [d], V. Siva [e], J.N. Cheerlin Mishma [f], S. Abul Kalam Azad [g], Y. Sheena Mary [h]

[a] Department of Chemistry, Muthayammal Memorial College of Arts and Science, Rasipuram, 637408, India
[b] Department of Physics, Muthayammal Memorial college of Arts and Science, Rasipuram, 637408, India
[c] Department of Chemistry, Thiruvalluvar Government Arts College, Rasipuram, 637 401, India
[d] Departamento de Química Farmacéutica y Orgánica, Facultad de Farmacia, Universidad de Granada, Campus de Cartuja s/n, Granada, 18071, Spain
[e] Department of Physics, Karpagam Academy of Higher Education, Coimbatore, 641021, India
[f] Department of Physics, Women's Christian College, Nagercoil, Tamil Nadu, India
[g] Department of Bio-Chemistry, Rajah Serfoji Government College Thanjavur 613005, India
[h] Department of Physics, FMN College, University of Kerala, Kollam, Kerala, India

ARTICLE INFO

Keywords:
Sitagliptin
Topological
Docking
MD simulation
Metal clusters

ABSTRACT

Sitagliptin is a medication used to manage type-2 diabetes. The present study investigates the experimental and theoretical results of Sitagliptin (SG). Density functional theory (DFT) calculations were used to determine optimized parameters at the B3LYP functional /6-31++G(d,p) basis set. In addition Time-dependent DFT is used to compute excited states of SG and SG-Ag_6 and predict UV spectra. The electronic properties of silver nano cages containing SG have exhibited a notable enhancement. Natural bond orbital (NBO) analysis was also used to determine charge transfer within the molecule and stabilization energy. Electronic properties such as molecular electrostatic potential (MEP), frontier molecular orbital (FMO) analysis of SG and SG-Ag_6 were investigated. The chemical significance of SG has been discussed using electron localization function (ELF) and local orbital locator functions (LOL) with contour images. Sitagliptin appears to have promise as a treatment for the chosen inhibitors, according to the docking binding affinities and the formation of a significant amount of hydrogen bonds. The molecular dynamics simulations were also performed using Gromacs 5.1.3 and discussed.

1. Introduction

In the pharmaceutical industry, chemists develop and select substances for biological evaluation. Molecular biologists in drug development must be more knowledgeable than organic chemists in order to anticipate problems and evaluate improvements. The chemist develops the drug project's hypothesis, which establishes its objectives [1–3]. Most organic materials, particularly natural products, contain heterocyclic rings. These rings allow for changes in molecular conformation, solubility, physical and chemical properties, pharmaceutical properties, and biological properties. Sitagliptin is used to treat type-2 diabetes as an anti-diabetic medication. Sitagliptin increases production and decreases excessive hepatic glucose production. It lowers alpha cell glucagon secretion. It was the first agent in this new class of drugs to be approved [4–6]. In 2006, it was permitted for medicinal use in the United States after being developed by Merck & Co [7].

Sitagliptin may be used as part of a combination therapy. There is a characteristic shared by all forms of diabetes mellitus. The body normally converts the sugars and carbohydrates absorbed into a unique sugar called glucose. The cells in our body are fed by glucose [8–10]. However, in order for the cells to absorb the glucose and utilize it as energy, there must be enough insulin, a hormone, in the bloodstream. Sitagliptin helps to inhibit DPP-4 (dipeptidyl peptidase) competitively. This enzyme degrades the digestive hormones GLP-1 and GIP, which are secreted after meals. They are able to boost insulin secretion and decrease glucagon release by the pancreatic alpha cells by blocking GLP-1 and GIP inactivation [10–13]. When compared to a placebo, sitagliptin has been demonstrated to reduce HbA1c levels by roughly 0.7 % points. When administered as a monotherapy, it performs somewhat worse than metformin. The significance of assessing the chemical

* Corresponding author.
E-mail address: venkateshindhuja@gmail.com (G. Venkatesh).

https://doi.org/10.1016/j.chphi.2024.100481
Received 20 December 2023; Received in revised form 15 January 2024; Accepted 16 January 2024
Available online 22 January 2024

stability of pharmaceuticals in the finished pharmaceutical products is emphasized in many guidelines [12–15]. It is an important method in molecular modeling and drug design. In diabetic use, the DPP-4 inhibitor can block the DDP-4 to attenuate GLP-1 degradation and prolong GLP-1 its action and sensitize insulin activity for the purpose of lowering blood glucose. Nonetheless the adverse effects of DPP-4 inhibitors severely hinder their clinical applications, and notably there is a clinical demand for novel DPP-4 inhibitors from various sources including chemical synthesis, herbs, and plants with fewer side effects [12–15]. It is generally recognized that active ingredients and excipients can interact, for instance, in a hydrolytic or oxidative manner [16]. Up to this point, not much study has been conducted on the chemical stability of sitagliptin in the presence of various excipients. Finding effective medications has captured the interest of numerous researchers worldwide. To prevent their toxicity and adverse effects on healthy cells, managing the selectivity and releasing rate of these medications can be thought of as the most challenging problem in the treatment of disorders.

One of the areas of active research in materials science, biophysics, chemistry, medicine, and nanotechnology is intermolecular interactions. Intermolecular interaction forces play a major role in the solvation and association process, influencing the structure, vibrational properties, electron density distribution, reactivity, and numerous other dynamic parameters of molecules. Studying the effects of solvation is typically very challenging due to the molecular nature of the solute-solvent interactions. These substances must therefore be examined at the molecular level [17–20]. One of the most common types of nanostructures is the cage, which produces a particular type of hollow spheroid with a distinctive shape. Since this approach can raise frequency by a million times, there has been a rise in interest in predicting the spectrum intensities that come from SERS when organic analytes bind to nano metal cages substrates. Chemistry and materials scientists have discovered that SERS works well for detecting chemicals in trace quantities and is valuable in biomedical and food applications. Using first principle calculations with compounds containing nano metal cages and the spectrum characteristics radiated by such interactions, the SERS effect is currently being investigated at the atomic level [21–23]. The creation of nanocarriers for disease medications relies heavily on nanotechnology. Due to their unique physical and chemical characteristics that enhance the immune system, nano drug carriers are regarded as a viable technique for the treatment of cancer [24–28]. Additionally, they can lessen side effects and increase the solubility and accumulation of medications in the target tumour locations. The precise prediction of information regarding molecular characteristics benefits greatly from DFT analysis [29–34].

A review of the literature shows the significance and restrict of the necessary evaluation of new drug molecules. The solvent effect, chemical reactivity, geometrical parameters, and spectral properties of SG and SG-Ag_6 have all been determined and discussed in the present study. Furthermore, electrostatic potential (MEP), frontier molecular orbitals (FMOs), and energy gaps have been constructed to better understand the electronic properties, nucleophilic and electrophilic sites of the compound under consideration. Thermal behaviors as well as thermodynamic properties have been determined. In addition, a molecular docking analysis was conducted to determine the binding potential of target molecules with protein DPP-4. The molecular dynamics simulations were performed in various media and discussed. It is an important method in molecular modeling and drug design.

2. Experimental study

The Sitagliptin (SG) was purchased from Sigma Aldrich and used throughout the assessment. The FT-IR spectrum of SG is obtained using a Perkin Elmer FT-IR instrument and KBr pellets. The UV-Vis spectra were captured using a Shimadzu UV spectrophotometer with 1.0 cm matched quartz lenses. The ^{1}H and ^{13}C NMR spectra were acquired at room temperature with the 400 MHz Bruker Avance III instrument and deuterated chloroform solvents.

2.1. Computational calculation

Density functional theory (DFT) is a set of techniques for quantum mechanical electronic structure calculations that have a wide range of applications in organic and main group molecules, as well as more complex systems [35–40]. Hence, all quantum computational calculations for SG and SGAg_6 were carried out using the DFT method with the B3LYP/6-31G++(d,p) basis set and the Gaussian 09 program [41]. The Molecular structure was visualized using the Gauss View 6.0 package. In addition, TD-DFT calculations were performed using optimized geometries to obtain information on the absorption properties of the excited and ground states with the same functional and level of theory. The vibrational wavenumbers were determined through the utilization of potential energy distribution (PED) calculations, employing the VEDA programme [42]. Furthermore, the analysis of the Electron Localization Function (ELF) and Local Orbital Localization (LOL) was conducted using the Multiwfn software [43].

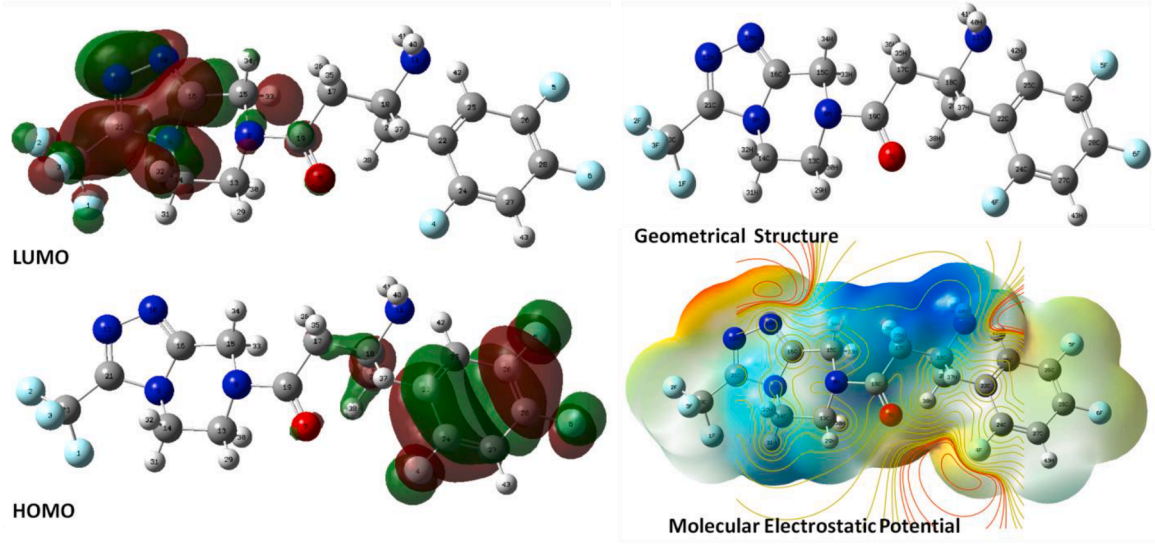

Fig. 1. FMO orbital, Geometrical and Molecular electrostatic potential of SG.

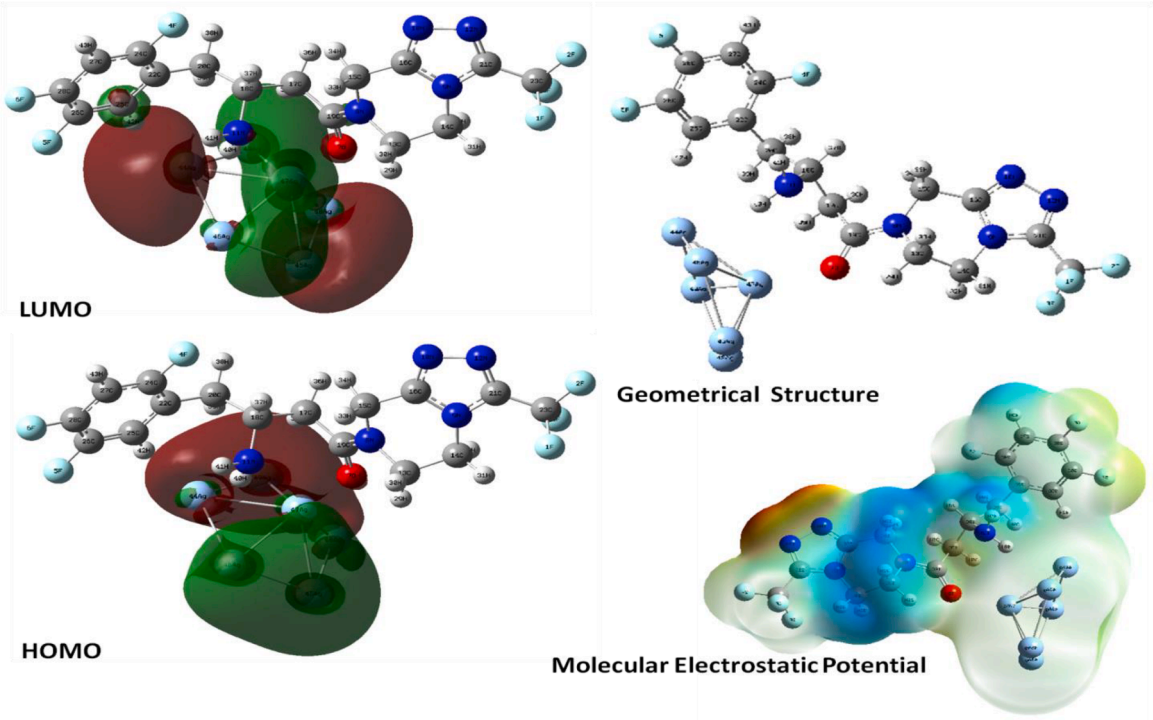

Fig. 1.1. FMO orbital, Geometrical and Molecular electrostatic potential of SG-Ag_6.

2.2. Molecular docking

Crystal structure of human depiptidyl peptidase IV (DPP-4) (PDB ID: 3W2T). This protein is mainly involved in type-2 diabetes [44]. BIOVIA Discovery studio [45] software was used in this molecular docking analysis. The previously reported protocol for docking study was used (https://pubs.rsc.org/en/content/articlehtml/2017/sc/c8ra01854e).

2.3. Molecular dynamics simulation

The molecular dynamics simulations have been carried out utilizing Gromacs 5.1.3 [46]. To parametrize the SG, the neutral and charged form of the molecule were submitted to Swissparam server (http://www.swissparam.ch/) [47]. Marvin software V 22.13 was used to predict the pKa of SG and to infer the most predominant specie at neutral pH (7) [48], where the primary amine group is protonated. Charged and neutral forms of SG were submitted into a cubic box of TIP3P water model or ethanol [49], respectively. The system was neutralizing by adding one chloride ion. The systems were reduced with the steepest descent technique for 50,000 steps. Additionally, equilibration was conducted for duration of 100 ps in the NVT ensemble at a temperature of 300 Kelvin. Subsequently, a second equilibration was performed using the NPT ensemble for 100 ps in order to attain a stable pressure and density for the system. The system was coupled to a bath with a constant pressure of 1 bar and a coupling time of $\tau P = 2$ ps. The electrostatic interactions have been intended using the Particle-Mesh Ewald (PME) technique, with a cut-off distance of 10 Å and a time step of 2 fs. A molecular dynamics (MD) simulation was conducted for duration of 20 ns. The MD simulation protocols utilized in prior studies were adhered to [50,51]. A total of 21 conformers were obtained from the production of molecular dynamics (MD) simulations, with each conformer retrieved at intervals of 1 nanosecond. Subsequently, all of the obtained structures were aligned to the reference structure at 0 nanoseconds using Discovery Studio v17R2 [46].

3. Results and discussions

3.1. Geometrical analysis

The SG and SG-Ag_6 geometrical structures (Figs. 1 and 2) and their parameters are listed in supplementary material Table S1. The calculated bond length of C23-F1, C23-F2, C23-F3, C24-F4, C26-F5 and C28-F6 are 1.34 Å, 1.33 Å, 1.35 Å, 1.33 Å, 1.33 Å and 1.33 Å. The bond length of N11-H40, N11-H41, N10-N12, C14-N9, C15-N8, C13-N8 and C18-N11 are 1.02 Å, 1.01 Å, 1.33 Å, 1.48 Å, 1.48 Å, 1.48 Å and 1.48 Å show that single bond characters. The bond lengths of C19-O7, C21-N12, and C16-N10 are 1.22 Å, 1.37 Å, and 1.37 Å, respectively, indicating double bond attributes. Furthermore C17-C18 has the highest bond length at 1.56 Å, while N11-H41 had the shortest bond length of 1.01 Å found in the present study. The calculated bond angle of F1-C23-F2, F2-C23-F3, F5-C26-C25, F5-C26-C28 and C22-C24-F4 are 104.7, 104.6, 119.3, 119.7 and 119.5°, respectively. In addition, bond angle of N9-C21-N12, N10-C16-N9, N8-C15-C16, C13-N8-C15 and C16-N9-C21 are 108.1, 108.5, 110.7, 113.6 and 105.1°. Alternatively, the bond angles of H29-C13-H30, H36-C17-H35, N8-C19-O7 and C17- C19-O7 are 107.1, 105.3, 118.4 and 123.1°. The highest bond angle of C23-C21-N12 is 126.2° and the smallest bond angle of F1-C23-F3 is 103.8° calculated in the present study. The highest dihedral angle for C25-C26-C28-F6 is 180.1°, while the smallest dihedral angle for C16-N10-N12-C21 is 0.1° calculated in the present study. The calculated dihedral angle of C22-C20-C18-N11, C18-C17- C19-N8, N8-C15-C16-N9, N8-C13-C14-N9, N9-C16-N10-N12 and N9-C12-N12-N10 are 72.50°, -172.46°, -14.47°, 47.83°, -0.069° and -0.838°, respectively. The dihedral angles of C22-C25-C26-C28 and C28-C26-C24-C22 are 0.303° and 0.152°, respectively, indicating that the aromatic ring has a sustained planar structure. F1-C23-C21-N12 and F3-C23-C21-N9 dihedral angles were determined as 120.7° and 60.81°, respectively, indicating the possibility of in-plane and out-plane bending modes. The bond length of Ag47-O7 was calculated as 2.31 Å. The bond angles Ag46-Ag44-Ag49, Ag46-Ag45-Ag48, Ag44-Ag46-Ag45, O7-Ag47-Ag44, O7-Ag47-Ag45, O7-Ag47-Ag46, O7-Ag47-Ag48, O7-Ag47-Ag49 were also calculated as 109.3, 108.7, 106.9, 126.6, 117.9, 118.1, 120.9 and 125.7°, respectively. The findings

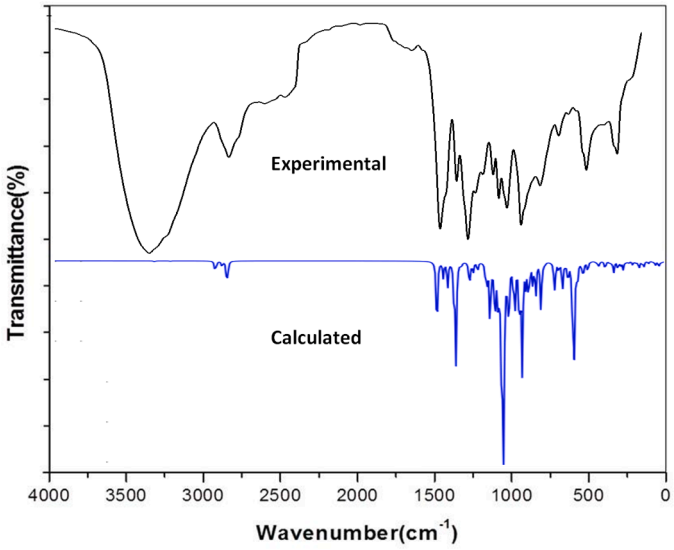

Fig. 2. Experimental and calculated vibrational spectra of Sitagliptin.

show that when sitagliptin nanocages are packaged, their physico-chemical properties significantly improved.

3.2. Vibrational Spectral analysis

The FT-IR spectra have been recorded and compared with calculated spectra and are shown in Fig. 3. The experimental CH stretching vibrational modes assigned at 3255, 3174, 3188, 3052, 2970, 2918 and 2850 cm^{-1}, which are agreed with the scaled bands of 3246, 3175, 3144, 3054, 3109, 3101 and 3104 cm^{-1} are, respectively (refer Table 1). The CH in-plane bending modes are assigned at 1296, 1222, 1164, 1121, 1062 and 1028 cm^{-1} and these values are well correlated with computed vibrations at 1298, 1219, 1167, 1125, 1073 and 1031 cm^{-1} respectively. The CH out-plane bending modes are arrived at 942, 728 and 688 cm^{-1} and the bands well correlated with computed vibrations at 946, 731 and 691 cm^{-1}. The symmetrical and asymmetric valence stretching vibrations (υNH) appear in a single broad band between 3500 and 3000 cm^{-1}. The experimental NH stretching vibration modes assigned to asymmetry and symmetry are found in 3624 and 3618 cm^{-1}, and the calculated bands are 3613 and 3503 cm^{-1}. The deformation vibration bands of NH_2 typically occur between 1600 and 1575 cm^{-1}. The NH_2 is found at 1627 cm^{-1}, which is well correlated with calculated bands at 1633 cm^{-1}, and the results are also well correlated with previous work [52,53]. The experimental C-C bending vibrational spectra assigned at 1528, 1472 and 1416 cm^{-1}, which are well correlated with calculated bands at 1531, 1485 and 1413 cm^{-1}. The CCC ring bending vibrational modes assigned at 1142 and 419 cm^{-1}, which are well correlated with calculated modes at 1139 and 414 cm^{-1}. The carbonyl stretching frequency is highly responsive to perturbations that affect the carbonyl group's characteristics, and its exact frequency is indicative of the carbonyl compound under investigation. Organic chemists regard this area as among the most crucial in the world. The stretching vibration band (C=O) is commonly found at 1850–1550 cm^{-1} ranges. In the present study, the stretching bond (υC=O) has been identified at 1568 cm^{-1}, while the band was computed at 1564 cm^{-1}. The experimental NC stretching vibrational spectra assigned at 1262, 1242 and 872 cm^{-1}, which is well correlated with calculated bands at 1266, 1243 and 877 cm^{-1} respectively. The experimental NCC vibrational spectra assigned at 568 cm^{-1}, which is well correlated with calculated bands at 565 cm^{-1}. The experimental CNC vibrational spectra assigned at 628 cm^{-1}, and simulated band indentified 625 cm^{-1}. The vibrational spectra were recorded in DMSO solvent, and the vibrational modes deviated slightly from previous literatures [54–56].

Table 1
Fundamental vibrational assessments of Sitagliptin.

S.No	Exp.	Cal.	IR Intensity	TED
1	3624	3613	0.71	ν_{asym}NH(99)
2	3618	3503	0.29	ν_{sym}NH(99)
3	3255	3246	4.53	νCH(99)
4	3174	3175	3.8	νCH(100)
5	3188	3144	0.37	νCH(91)
6	-	3123	0.1	νCH(97)
7	-	3112	0.04	νCH(95)
8	-	3086	1.34	νCH(97)
9	3052	3054	2.03	νCH(98)
10	-	3017	5.31	νCH(96)
11	-	3117	2.31	νCH(96)
12	-	3115	5.49	νCH(92)
13	2970	3109	7.29	νCH(99)
14	2918	3101	6.05	νCH(98)
15	2850	3104	4.95	νCH(96)
16	1627	1633	71.51	$_{roc}$HNH(85)
17	-	1619	14.19	τHNCC(12)
18	-	1589	25.05	νCC(57)
19	1568	1564	38.03	νOC(74)
20	1528	1531	88.45	νCC(55)
21	1472	1485	3.64	νCC(26)
22	-	1484	6.6	σCCC(11)
23	1448	1443	2.52	σNCN(11)
24	-	1434	13.5	γHCH(21)
25	1416	1413	4.63	νCC(43)
26	-	1412	5.67	γHCC(31)
27	-	1382	8.87	νNC(12)
28	-	1328	10.54	γHCH(25)
29	-	1322	3.95	γHCH(61)
30	-	1316	15.53	νCC(10)
31	1296	1298	53.22	γHCH(79)
32	-	1294	6.44	γHCH(81)
33	-	1279	4.21	νNC(11)
34	1262	1266	16.58	νNC(17)
35	-	1263	14.53	τHCNC(11)
36	1256	1258	22.76	τHCNC(11)
37	1242	1243	17.5	νNC(19)
38	-	1239	16.4	σCCC(10)
39	-	1235	11.78	γHCN(14)
40	1222	1219	81.42	γHCC(19)
41	-	1207	80.22	τCCCH(12), νNC(10)
42	-	1205	43.79	τHCNC(22)
43	-	1202	94.69	σCCC(13), γHCC(10)
44	-	1194	17.04	σCCC(12)
45	-	1177	11.14	σCCC(31), γHCC(10)
46	1164	1167	58.28	γHCC(15)
47	1142	1139	14.13	σCCC(64)
48	1121	1125	35.26	γHCC(12)
49	-	1122	12.18	βHCCC(15)
50	-	1096	35.62	σHCN(29)
51	-	1093	12.97	σCCC(14), σHCN(11)
52	-	1086	17.66	τHCCN(16), σCCC(10)
53	1062	1073	100	γHCC(63)
54	-	1049	19.05	σCCC(14), σHCN(11)
55	1028	1031	28.95	γHCC(15)
56	-	1021	9.25	σCCC(29)
57	-	1000	19.89	σCCC(10)
58	-	981	6.52	νNC(12), σCCC(10)
59	-	979	25.19	σCCC(22), νNC(10)
60	942	946	19.94	βHCCC(52)
61	-	943	27.25	γHNC(25)
62	-	932	1.75	σCCN(15)
63	-	918	2.14	σCCC(47), σCNC(10)
64	872	877	0.39	νNC(12), σCNC(17)
65	-	855	7.62	σCCC(73)
66	-	848	23.91	σCCC(52)
67	-	823	7.39	σCCC(10)
68	799	796	28.4	τNCCN(10)
69	-	775	2.35	σNCC(11)
70	-	758	17.85	σCNC(30)
71	728	731	6.17	βHCCC(20)
72	-	728	18.06	τHCCN(11)
73	-	723	30.98	σCNC(11)
74	-	715	86.01	σNCN(31), σNCC(10)

(continued on next page)

Table 1 (*continued*)

S.No	Exp.	Cal.	IR Intensity	TED
75	-	693	15.88	σCCC(14)
76	688	691	3.28	βHCCC(14)
77	-	665	1.88	βHCCC(79)
78	-	657	6.81	τCCCC(15)
79	-	649	7.13	σNCC(10)
80	628	625	1.6	σCNC(17)
81	-	621	7.99	σCCC(37)
82	-	604	0.21	τCNCN(59)
83	568	565	1.06	σNCC(14)
84	-	551	2.09	σOCC(12)
85	542	543	3.73	τCCCC(31)
86	-	504	4.21	τCCNC(56), τCCCC(10)
87	-	498	2.77	σCCC(10)
88	-	469	1.88	τCCCC(57)
89	-	456	1.1	σCCC(19), τCNCN(10)
90	-	442	10.7	τOCNC(26)
91	419	414	7.13	σCCC(13)
92	-	401	0.13	σCCC(10)
93	-	394	3.7	σCCC(14), τCNCN(10)
94	-	377	7.43	τCNCN(44)
95	-	363	1.14	σCNC(14)
96	-	349	0.98	τCCCC(10)
97	-	337	1.51	σCCN(15), σCNC(11)
98	-	311	3.47	σCCC(11)
99	-	291	1.41	σCNC(38), τCNNC(14)
100	-	283	0.63	τHCNC(14)
101	-	270	1.41	σCCC(14), τCNCC(10)
102	-	266	5.59	τHNCC(69)
103	-	247	1.39	τCCCC(36)
104	-	235	5.59	τCCCN(13)
105	-	224	0.23	σCCC(52), τCCCC(16)
106	-	202	2.28	σCCN(45)
107	-	173	0.89	τCCCC(21)
108	-	155	4.23	τCCCN(16), τHCNC(11)
109	-	133	2.52	τCNNC(14)
110	-	129	2.72	τHCCN(27), τHNCC(11)
111	-	118	1.42	τCNCC(13)
112	-	105	0.99	σCCN(23), τCNCC(10)
113	-	94	1.09	σCCN(37)
114	-	87	1.9	σCCC(16), σCCN(11)
115	-	73	1	τCCCC(14)
116	-	68	0.16	τCNNC(52), τCNCC(10)
117	-	52	0.27	τCNCC(54), τHCNC(11)
118	-	42	5.23	σNCC(70)
119	-	38	0.31	τNCCC(19)
120	-	31	0.89	τCCNC(42), τCCNC(11)
121	-	27	0.16	τCCCC(56)
122	-	25	1.67	τCNCC(79), τHCNC(11)
123	-	19	38.38	τCCNC(70)

3.3. NMR spectra

The ^{1}H & ^{13}C NMR spectra (Figs. S1 and S2) are compared with calculated NMR data and listed in Table S2. SG aromatic carbon of C19, C21, C16, C24, C26, C28, C22 and C25 chemical shifts are observed (calculated) at 175.01 (181.39), 159.66 (153.97), 158.94 (153.31), 154.37 (146.69), 151.95 (136.05), 138.29 (135.91), 121.97 (124.26) and 116.98 (113.56) ppm respectively. The alkyl carbon of C15, C18, C17, C13, C14 and C20 chemical shifts found at 40.63 (31.10), 40.42 (29.95), 40.21 (29.17), 40.00 (26.62), 39.79 (25.21) and 39.38 (19.03) ppm respectively. The aromatic ring protons H42 and H43 chemical shifts found at 7.64 (7.55) and 7.63 (7.42) ppm, respectively. The amino protons H42 and H43 chemical shifts found at 7.64 (7.55) and 7.63 (7.42) ppm respectively. And also the alkyl protons of H34, H29, H31, H33, H37, H32, H38, H30, H35, H36 and H39 are found at 3.43 (3.41), 3.41 (2.95), 3.39 (2.79), 3.38 (2.73), 2.52 (2.34), 2.51 (2.31), 2.44 (2.18), 2.48 (2.29), 1.20 (1.31), 1.11 (1.24), 1.03 (1.21) and 1.01 (1.19) ppm, respectively. The experiment NMR spectral values are well correlated with calculated data in the present study. The results may be support for higher study in various fields.

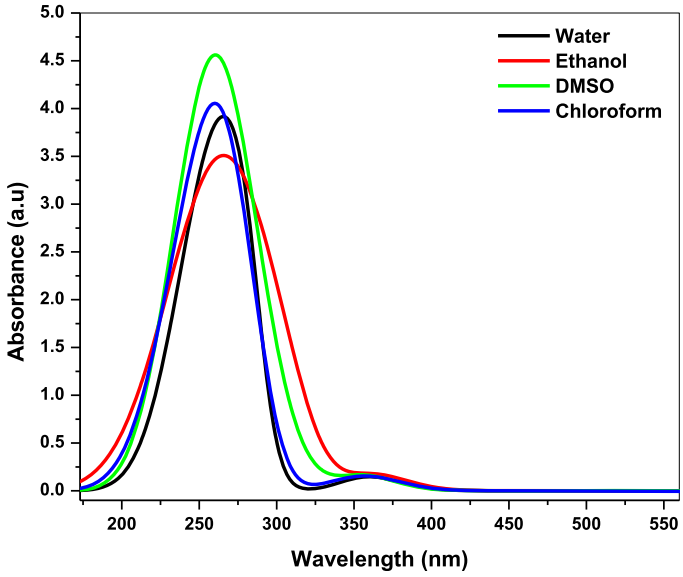

Fig. 3. Experimental UV spectra of Sitagliptin

3.4. Absorption and physico chemical Properties

The SG UV spectra were acquired at ambient temperature, encompassing the wavelength interval of 200–800 nanometers. By means of electronic transitions from bonding orbitals to anti-bonding orbitals, UV and visible light absorption reveals information regarding the molecule's structure [54–56]. In the present study, 272, 274, 269 nm (Water, DMSO, and Chloroform) and 361, 364 & 366 nm peaks reveal that π→π* and n→π* electronic transitions occurred in the SG molecule (Fig. 4). In addition, the ethanol medium exhibits electronic transitions at wavelengths of 281 and 378 nm. These transitions are influenced significantly by the protic nature of ethanol as a solvent, which plays a prominent role in comparison to other solvents [54–56]. The absorption SG also calculated with TD-DFT/B3LYP method by the 6-31++G (d,p) basis set using ground state optimized geometry and is shown in Fig. S3. The electronic characteristics of sitagliptin silver nanocage have been significantly improved (see Fig. 5). The calculated absorption wave lengths for the gaseous and aqueous states are 579.24 nm and 583.95 nm, respectively. In order to study the nature and energy of electronic changes the low-lying excited state transition has been calculated. Table 2 lists the calculated absorption wavelengths for SG and SG-Ag6, as well as their important electronic properties. The results provide clear evidence of the influence of solvent effects on drug bioavailability before and after consumption by alcohol drinkers. HOMO, LUMO energy levels and spatial electron density distributions are important criteria for decisive on photo physical and optoelectronics properties of materials. The HOMO-LUMO energy provides insights into the reactivity of the molecule as well as the light that is absorbed or transmitted. The electron density plot of the SG such as HOMO and LUMO are presented in Fig. 1. The HOMO is occupied in aromatic ring, while LUMO is occupied the triazol ring and oxygen atom. The Table 3 represents the physico chemical parameters it revels the nature of molecules. The utilization of MEP holds greater significance in establishing a correlation between drug activity and MEP values due to its qualitative nature as opposed to a quantitative approach.

One of the potential advancement in applications utilizing MEP involves the incorporation of specific parameters aimed at reducing the presence of variability in the perception of similarity. In order to visually depict the sizes, contours, and distribution of positive, negative, and neutral potential regions, the term molecular electrostatic potential is implemented [57–61]. This information is highly beneficial in ascertaining the location of the binding receptor that is significantly more

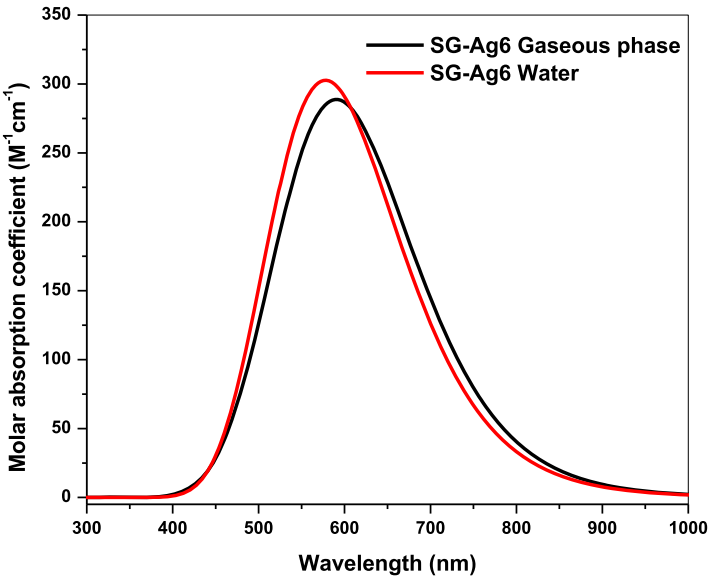

Fig. 4. Calculated UV spectra of SG-Ag_6.

Table 2
Absorption energy and molecular orbital contribution of Sitagliptin.

Solvent	λ_{max}	Absorption energy (eV)	Oscillator strength (f)	MO Contribution
Gaseous	363.46	2.6752	0.7412	HOMO→LUMO (99 %)
	266.64	3.3816	0.0091	HOMO→L+1 (85 %) H-3→LUMO (3 %), H-1→LUMO (9 %)
	263.34	3.4123	0.0195	HOMO→L+2 (55 %), HOMO→L+2 (41 %), H-1→LUMO (1 %)
SG-Chloroform	360.84	2.6904	0.0148	HOMO→LUMO (98 %)
	275.68	3.3003	0.0016	H-2→LUMO (81 %), H-1→LUMO (11 %)
	266.19	3.3858	0.1184	H-1→LUMO (64 %), HOMO→L+2 (22 %)
SG-Water	363.46	2.6752	0.0086	HOMO→LUMO (99 %)
	266.64	3.3816	0.0009	H-2→LUMO (15 %), H-1→LUMO (66 %), HOMO→L+3 (12 %)
	263.34	3.4123	0.0195	H-1→LUMO (66 %), HOMO→L+1 (21 %), HOMO→L+2 (13 %)
SG-Ethanol	371.55	2.8746	0.0097	HOMO→LUMO (99 %)
	271.24	3.6473	0.0011	H-1→LUMO (16 %), H-2→LUMO (55 %), HOMO→L+1 (22 %)
	264.96	3.9865	0.0193	H-1→LUMO (32 %), HOMO→L+1 (44 %), HOMO→L+2 (16 %)
SG-DMSO	364.51	2.6749	0.0034	HOMO→LUMO (98 %)
	267.14	3.3771	0.0011	H-2→LUMO (66 %), H-1→LUMO (22 %), H-3→L+1 (4 %),
	263.63	3.4097	0.0199	H-5→LUMO (15 %), H-2→LUMO (51 %), H-1→LUMO (13 %)
SG-Ag6 (Gaseous)	583.95	2.1232	0.3124	H-1→L+1 (66 %), HOMO→LUMO (30 %), HOMO→L+1 (14 %), H-1→LUMO (8 %), H-1→L+2 (4 %)
	574.94	2.1565	0.0441	H-1→L+1 (40 %), H-1→L+2 (30 %), HOMO->L+2 (28 %)
	553.94	2.2383	0.0018	H-1→LUMO (27 %), HOMO→LUMO (25 %), HOMO→L+1 (25 %)
SG-Ag6 (Water)	579.24	2.3431	0.7157	HOMO→LUMO (70 %), HOMO→L+1 (18 %), H-1→LUMO (5 %),
	568.16	2.5545	0.0544	H-1→L+2 (40 %), H-1→L+3 (30 %), HOMO→L+1 (28 %)
	548.51	2.4331	0.0048	H-1→LUMO (29 %), HOMO→LUMO (22 %), HOMO→L+1 (21 %)

Table 3
Physico chemical parameters of Sitagliptin.

Solvent	HOMO (eV)	LUMO (eV)	IP (eV)	EA (eV)	ΔE (eV)	χ (eV)	μ (eV)	η (eV)	σ (eV)	ω (eV)	ε (eV)	ω+(eV)
SG-Gaseous	-5.032	-2.359	5.032	2.359	2.673	-3.695	-3.695	1.336	0.748	5.109	0.196	1.526
SG-Chloroform	-5.095	-2.407	5.095	2.407	2.687	-3.751	-3.751	1.344	0.744	5.235	0.191	1.572
SG-Water	-5.048	-2.345	5.048	2.345	2.703	-3.696	-3.696	1.352	0.740	5.055	0.198	1.493
SG-Ethanol	-5.039	-2.367	5.039	2.367	2.672	-3.703	-3.703	1.336	0.748	5.131	0.195	1.535
SG-DMSO	-5.034	-2.361	5.034	2.361	2.673	-3.698	-3.698	1.336	0.748	5.116	0.195	1.528
SG-Ag_6 (Gaseous)	-4.461	-1.781	4.461	1.781	2.680	-3.121	-3.121	1.340	0.746	3.634	0.275	0.938
SG-Ag_6 (DMSO)	-4.468	-1.791	4.468	1.791	2.677	-3.129	-3.129	1.339	0.747	3.658	0.273	0.948

probable. The N, F, and O atoms, as well as the phenyl ring, exhibited an electrostatic negative potential, as evidenced by the presence of red and yellow colors. The most electropositive elements were identified in close proximity to the hydrogen atoms. Nevertheless, this implies that the compound's biological activity demonstrates a significant interaction with the targets. Following the adsorption process involving SG-Ag_6, a redistribution of potential values occurs. Specifically, the hydrogen atom of the NH group exhibits a shift towards a bluish hue, while the red and yellow colors associated with the oxygen atoms and phenyl ring respectively diminish, resulting in a slight yellow coloration observed over the Ag_6 cluster. The findings indicate that the chemical reactivity of sitagliptin was enhanced subsequent to its nanocage.

Table 4
Dipole moment, solvation energies and minimal energy of SG and SG-Ag_6.

Name of the solvent	Minimal energies (a.u)	Solvation energies (kJ/mol)	Dipole moment (Debye)	Polarizability (a.u.)
SG-Gaseous	-1564.5537	-	1.9537	250.25
SG-Chloroform	-1564.5454	-5.22	2.371	254.88
SG-Water	-1564.5433	-6.53	2.074	287.72
SG-Ethanol	-1564.5374	-10.27	2.356	267.37
SG-DMSO	-1564.5433	-6.54	2.079	287.22
SG-Ag6-Gaseous	-32616.3007	-	9.9784	422.16

Table 5
Thermodynamic properties of Sitagliptin.

Name of the solvent	ΔE (Kcal/Mol)	ΔH (Kcal/Mol)	ΔG (Kcal/Mol)	S (Cal/Mol-Kelvin)
SG-Gaseous	212.2801	212.8725	168.6281	148.39
SG-Chloroform	224.7868	212.8725	168.6281	156.53
SG-Water	212.3084	212.902	168.2986	149.61
SG-Ethanol	221.3964	225.3811	178.0381	158.79
SG-DMSO	212.3115	212.9038	168.2773	149.68
SG-Ag6 (Gaseous)	204.0065	204.5418	143.7615	203.861

Table 6
The second order perturbation theory analysis results of the fock matrix in NBO basis of Sitagliptin.

Donor (i)	Type	Acceptor (j)	Type	$E^{(2)}$[a]	E(j) – E(i)[b]	F(i,j)[c]
F1-C23	π	F3-C23	π*	1.65	1.08	0.039
F2-C23	π	F1-C23	π*	1.26	1.12	0.035
O7-C19	π	N8-C15	π*	2.34	1.33	0.05
N8-C13	π	C17-C19	π*	2.61	1.11	0.048
N9-C21	π	N9-C16	π*	2.43	1.25	0.05
N9-C21	π	C15-C16	π*	4.26	1.23	0.065
N10-N12	π	N9-C21	π*	1.49	1.18	0.038
N10-N12	π	C15-C16	π*	5.91	1.16	0.074
N10-C16	π	N12-C21	π*	14.67	0.3	0.063
N12-C21	π	N9-C14	π*	3.55	1.15	0.057
N12-C21	π	N10-C16	π*	11.32	0.31	0.056
C17-C18	π	N8-C19	π*	3.21	1.02	0.052
C17-C18	π	C20-C22	π*	2.18	1.01	0.042
C17-C19	π	N8-C13	π*	3.87	0.94	0.054
C20-C22	π	C22-C25	π*	2.96	1.18	0.053
C21-C23	π	N12-C21	π*	2.68	1.26	0.052
C22-C24	π	C25-C26	π*	20.32	0.28	0.068
C22-C24	π	C27-C28	π*	21.46	0.27	0.069
C24-C27	π	C22-C24	π*	4.35	1.29	0.067
C25-C26	π	C22-C24	π*	18.19	0.29	0.066
C25-C26	π	C27-C28	π*	22.4	0.28	0.072
C27-C28	π	C22-C24	π*	19.53	0.29	0.069
C27-C28	π	C25-C26	π*	18.81	0.29	0.068
C27-C28	π	C25-C26	π*	312.96	0.01	0.082
C17-H36	π	O7-C19	π*	4.01	0.51	0.043
F1	LP	F2-C23	π*	10.94	0.56	0.07
F1	LP	F3-C23	π*	9.89	0.53	0.066
F3	LP	F1-C23	π*	10.08	0.53	0.066
F3	LP	F2-C23	π*	10.91	0.56	0.07
F5	LP	C25-C26	π*	17.06	0.4	0.08
F6	LP	C27-C28	π*	18.05	0.39	0.082
O7	LP	C17-C19	π*	17.66	0.62	0.095
N8	LP	O7-C19	π*	65.71	0.25	0.116
N8	LP	O7-C19	π*	65.71	0.25	0.116
N9	LP	N10-C16	π*	47.09	0.27	0.104
N9	LP	N12-C21	π*	44.57	0.27	0.103

[a] E(2) = Stabilization energy of hyper conjugative interaction
[b] Energy difference between the donor (i) and acceptor (j) NBO orbitals
[c] F(i,j) is the Fock matrix element between i and j NBO orbitals

3.5. Solvation effects

The solvation free energy of the SG drug is determined by various solvents such as water, ethanol (a protic solvent), DMSO (an aprotic solvent) and chloroform (a neutral solvent) [62]. Solvation free energy (Table 4) values for the SG are -5.22, -6.53, -10.27 and -6.54 kJ/mol. The results suggest that ethanol solvent exhibit greater effectiveness, primarily attributed to their higher solvation energy. Furthermore, these results provide additional support for the investigation of the biological properties of SG. The minimal energies of SG and SG-Ag_6 cluster are, -1564.5537 and -32616.3007 Hartree, the values suggesting a chemisorption process. The calculated thermodynamical parameters of ΔE, ΔH, ΔG, ΔS are listed in Table 5 and these results of adsorption are spontaneous and exothermic. The dipole moment and polarizability of SG are dramatically to higher values after adsorption with SG metal clusters. This enhancement shows the strong interaction with metal following a chemisorption process. The results clearly show that future drug design can be aided by adjusting the adsorption parameters of nanocaged sitagliptin.

3.6. Natural bond orbital analysis

NBO study is essential to the chemical clarification of hyperconjugative and charge transfer interactions across the molecular structure [63,64]. Table 6 displays the results of a second-order perturbation theory examination of the Fock matrix in NBO, which indicates the intra-molecular interactions. The SG is subjected to NBO analysis, which revealed the presence of significant electron D and A orbitals. In the present study, important interactions of F1-C23→F3-C23, O7-C19→ N8-C15, N10-C16→ N12-C21, N12-C21→ N10-C16, C22-C24→ C25-C26, C22-C24→ C27-C28, C25-C26→ C22-C24, C25-C26→ C22-C24, C25-C26→ C27-C28, C27-C28→ C22-C24, C27-C28→ C25-C26, C17-H36→O7-C19 stabilization energy are 1.65, 2.34, 14.67,11.32, 20.32, 21.46, 18.19, 19.53, 22.4, 19.53, 312.96, and 4.01 kcal/mol.

3.7. Electron-hole analysis

Studying electrons and holes can yield valuable insights into the properties of electron excitation [65]. The primary focus of research on electron-hole systems is exclusively directed towards the excited states, despite the fact that the majority of electronic transitions occur in both ground state and excited states. The analysis of electron and hole distribution for three excited states was conducted using Multiwfn 3.4.1 software [66]. Three excited levels of the substance were depicted in Fig. 6 with the distribution of the electron-hole pair. The depiction of hole configuration is represented by the colour blue, while the configuration of electrons is represented by the green color. Table 7 presents the numerical values pertaining to the overlap of electron-hole distribution, charge transfer length, r index, and excitation energy for various excitation modes observed in the gaseous state. In the first excited state, N12, N10, N9, F4, as well as certain carbon and hydrogen atoms, exhibit a configuration wherein they are encompassed by vacancies. Conversely, in the second and third excited states, N8, C18, O7, H35, H36, and C18 atoms possess an arrangement where they are encircled by electrons. Each of the three excited states exhibits a distinct electron distribution across the carbon-hydrogen (C-H) atoms within the phenyl ring. The observed charge transport distance exhibits a significant increase during the subsequent excitation phase. Furthermore, the value of

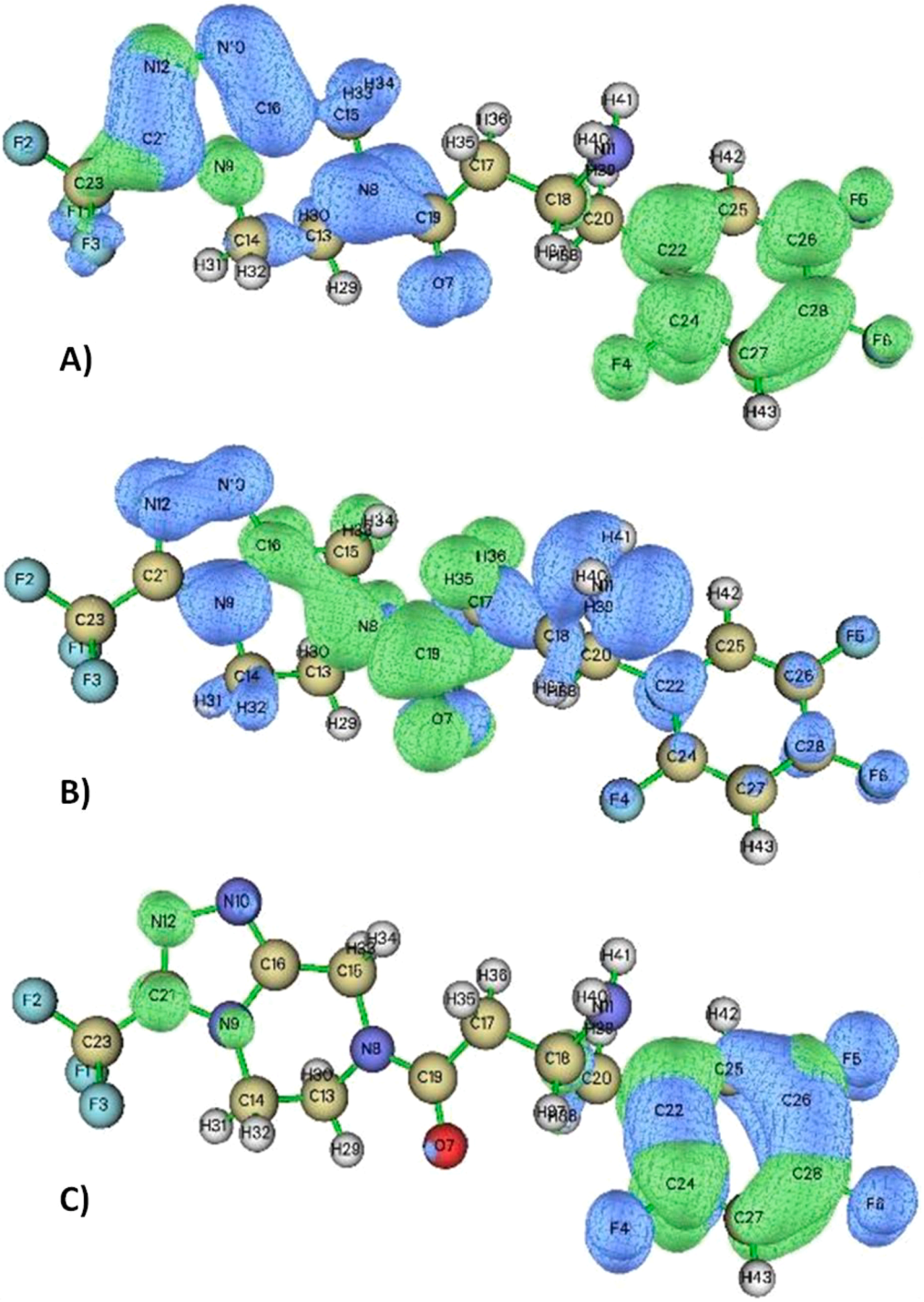

Fig. 5. Spreading of electron-hole pair over the material for three excited states in gas phase.

Table 7
Excitation energy (E), D index, Δ_r index, t index for different excited states of Sitagliptin in gaseous phase.

Parameters	First excited state	Second excited state	Third excited state
Excitation energy E (eV)	5.396	5.489	6.288
Charge transfer length D index (A°)	2.011	5.032	0.869
Δ_r index (A°)	3.592	6.763	1.613
t index (A°)	-0.255	1.534	-1.783

r is found to be higher for the same function, indicating that the second excitation mode is associated with a notable excitation of charge carriers.

3.8. ELF and LOL analyses

Weak interactions play a significant role in many physical, chemical, and biological processes. They can be used in a variety of applications, including hydrogen storage for renewable energies [67–69]. Reduced density gradient is an efficient and widely used technique for analyzing weak interactions such as repulsive interactions, van der Waals

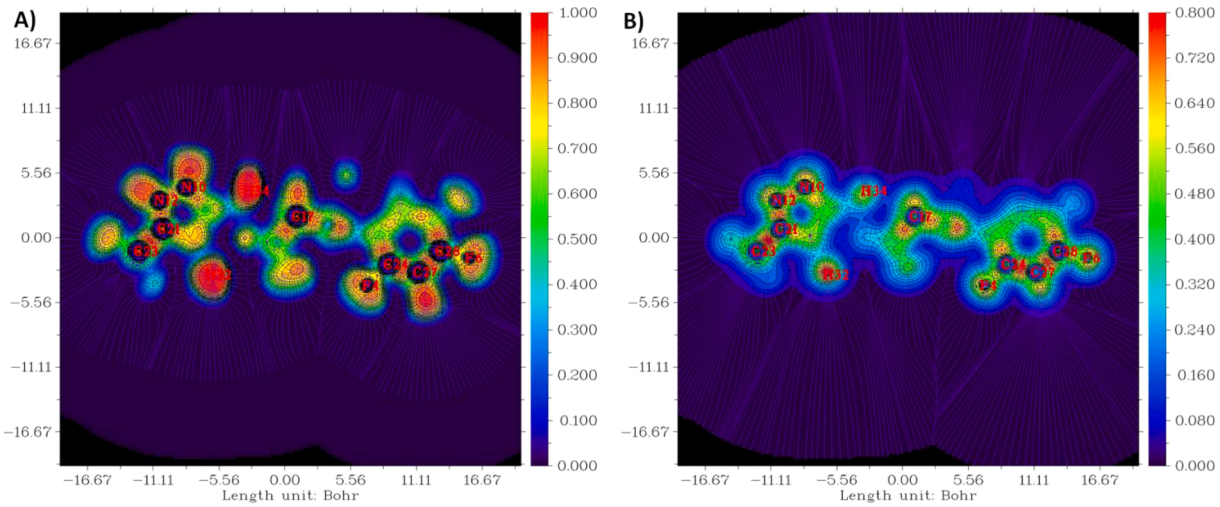

Fig. 6. (A, B): ELF (A) and LOL (B) maps for the gas phase.

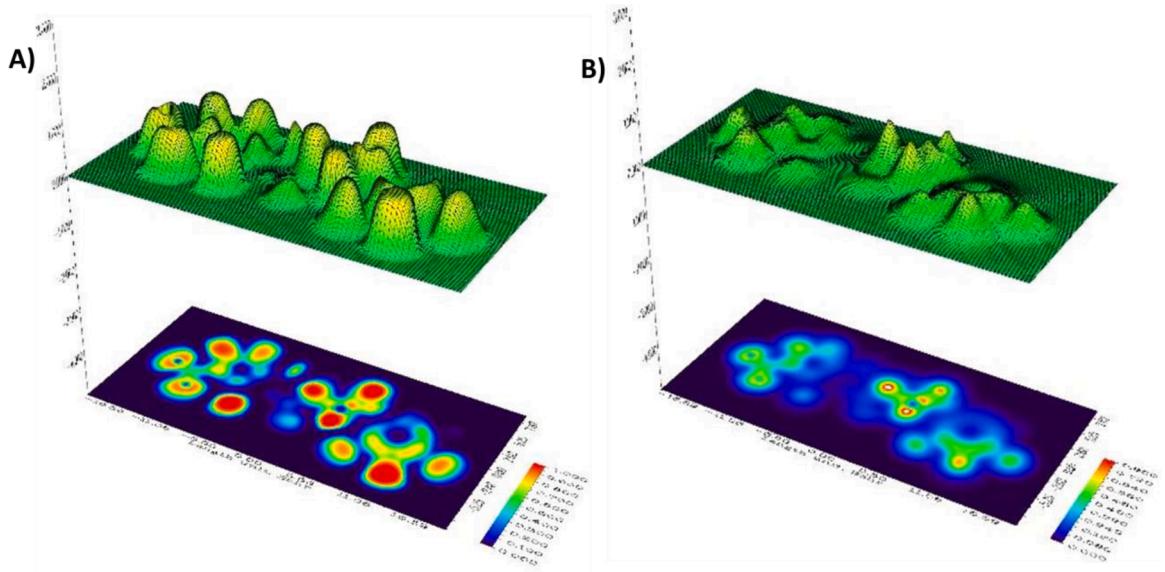

Fig. 7. ELF (A) and LOL (B) projection plot.

interactions, and hydrogen bonds that employs a simple color code. Johnson et al. [66] introduced the charge density, which serves as the foundation for the RDG approach. It demonstrates how the electron dispersion's neutrality is compromised [66,70–72]. The density of electrons decreases exponentially as distance from the particle increases, and as a result, RDG will be very valuable [73]. The presence of minimal RDG values, approaching zero, can be attributed to the formation of bonds with covalent and non-covalent relationships [74]. The representation of the following value of the Hessian (the second derivative) of the electron density (λ_2) q can serve as an indicator for discerning the nature of interconnections within the chemical system. Sign (λ_2) $>$ 0, (λ_2) $<$ 0, and (λ_2) $=$ 0 are graphic representations of the repelling, attractive, and Vander Waals (VDW) attractions, respectively. The color-filled RDG map and scatter map of the header composite [67] were generated using Multiwfn 3.8, as illustrated in Figs. 7 and 8. The NCI is surface diagram is visualized in 3D spatial isosurfaces in Fig. 9. The colour spectrum presented here illustrates molecular interactions characterized by attraction (non-covalent), repulsion (steric), and neutrality (van der Waals). The van der Waals interactions between are seen between hydrogen bond interactions huge amounts of green patches, intense hydrogen bond interactions are visible as blue spots, and repulsive steric forces are visible as red spots over the ring system. The research study contributed to the understanding of sitagliptin's properties and facilitated subsequent investigations.

3.9. Molecular docking

Random ligand conformations are generated from the initial ligand structure through high-temperature molecular dynamics (CHARMm), followed by random rotations. The random conformations are refined by grid-based (GRID1) simulated annealing and a final grid-based or full force field minimization [44]. The CDOCKER binding interaction of the Sitagliptin in the binding site with human depiptidyl peptidase IV (DPP-4) is – 32.741 Kcal/mol. In Sitagliptin binding analysis, Glu205, Tyr547, Arg125, Tyr662, Ser630 has showed the six strong H-bond with -NH_2, F, N, respectively. The active site Val711, Trr662 forms the Alkyl and Pi-Alkyl interaction with -CF_3 group. The other Phe357, Asn710, Ser 209 and Arg358 form the Van der Waals interaction with the Sitagliptin drug (Fig. 10).

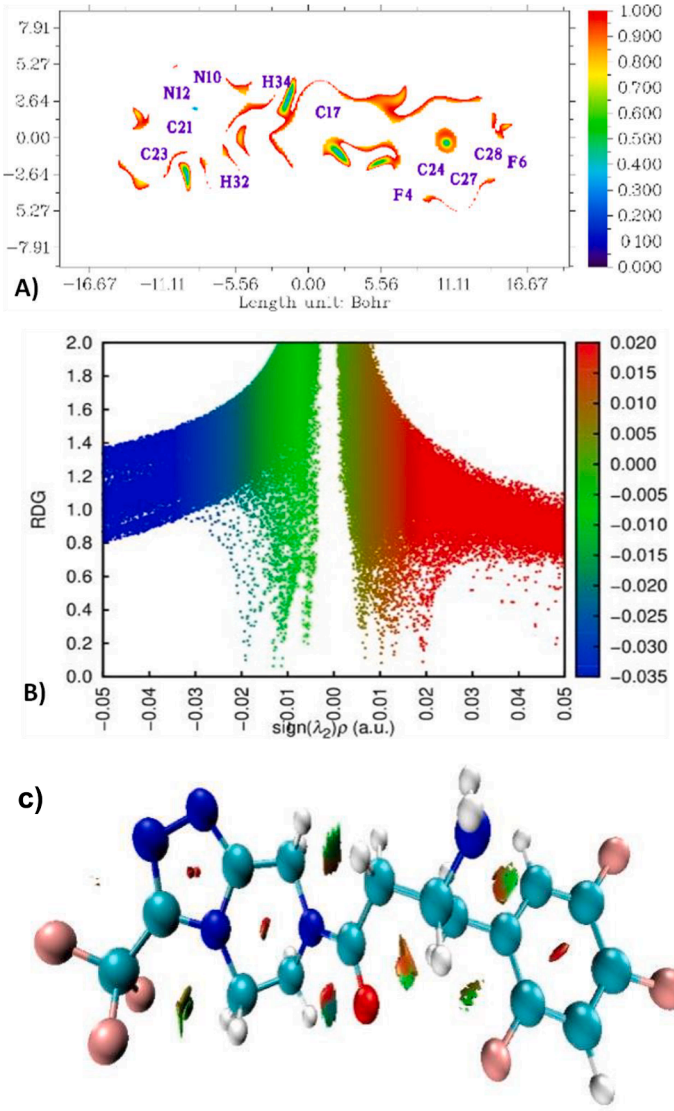

Fig. 8. (a, b): RDG Plots versus the electron density ρ multiplied by the sign of λ_2 in gaseous phase (c): 2D scatter and Isosurface density plots illustrating the non-bonded interactions of Sitagliptin.

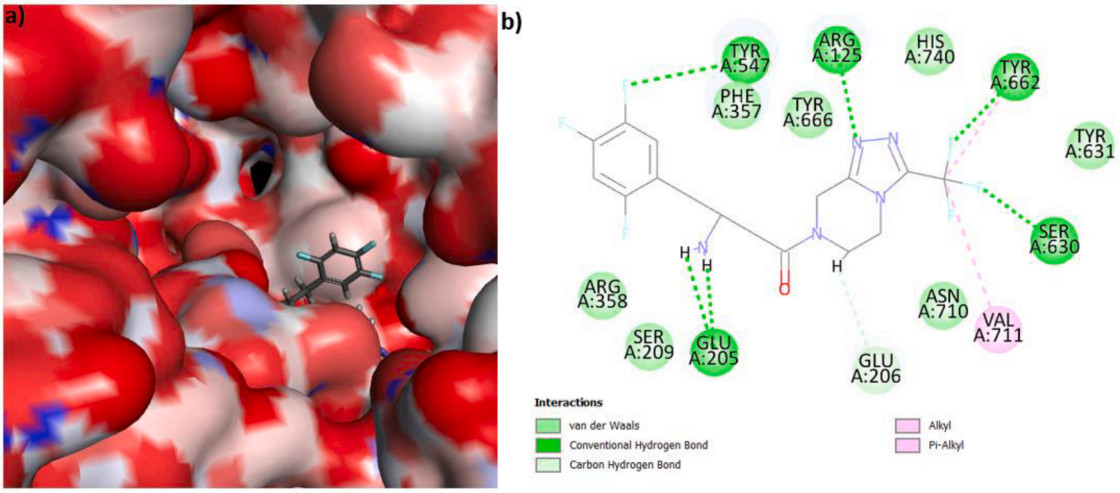

Fig. 9. a) 3D and b) 2D interaction of the Sitagliptin with human depiptidyl peptidase IV (DPP-4).

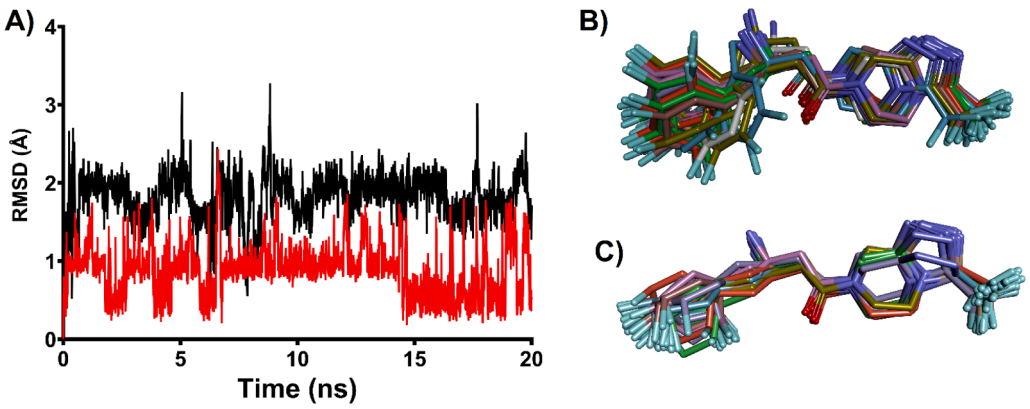

Fig. 10. A) RMSD of the charged and neutral SG embedded in water (black line) and ethanol (red line). Structural changes observed in SG molecule during MD simulation in B) water and C) ethanol. Conformations were sample at 1ns from 0ns to 20ns.

3.10. Molecular dynamic simulation

SG neutral and charged species were submitted to 20 ns of MD simulation embedded in ethanol or water box, respectively, to study the structural stability of the system in different solvents. From RMSD (Fig. 11A), charged SG in water showed greater RMSD than SG in ethanol which indicate more structural variation of SG in water environment than in ethanol. A visual inspection of the conformers obtained from MD simulation at regular intervals of 1ns can validate these results (Fig. 11). Comparing the conformers of SG in water (Fig. 11B) versus the ones in ethanol (Fig. 11C), when SG was embedded in water the trifluoro phenyl ring showed higher mobility while in ethanol it was more stable, this could be because it might be stabilized by hydrophobic interactions with the ethanol aliphatic portion. Additionally, the amines, nitrogen of the triazole moiety and carbonyl group form hydrogen bond with the alcohol group. The previously stated quantum calculations regarding the stability of the protonated SG are consistent with these results.

4. Conclusion

The vibrational spectroscopic characteristic of sitagliptin is examined in the present study utilizing FT-IR, UV-visible and NMR spectroscopic methods. Natural bond orbital analysis was performed to determine charge transfer in terms of "donor acceptor" within the molecule. The molecular electrostatic potential has been employed to predict the behaviour of SG reactants in electrophile-nucleophile reactions. The results obtained support the presence of hydrogen-bond interactions occurring within the molecules. The frontier molecular orbitals, calculated using the TD-DFT approach, are determined in the gas phase, water, and methanol solutions to explain charge transfer interactions. The electronic properties of silver nano cages containing sitagliptin have been significantly enhanced. RDG and ELF analyses were used to confirm the existence of these non-covalent interactions. Docking calculations were performed using the interaction between sitagliptin and complexes. The results show that the selected drug can be a good inhibitor of Glu205, Tyr547, Arg125, Tyr662, and Ser630, as it has a significant total energy score, making it an important candidate to study. The binding interaction between Sitagliptin and human dipeptidyl peptidase IV (DPP-4) in the binding site had been calculated to be -32.741 Kcal/mol. The conformers of SG in water versus those in ethanol, when SG was embedded in water, the trifluoro phenyl ring showed greater mobility, whereas in ethanol it was more stable, which could be due to hydrophobic interactions with the aliphatic portion of the ethanol, as revealed in the present study.

Access to information and materials

Given that no datasets were generated or examined in the context of this article, the concept of data sharing is not relevant.

Funding

The authors' submitted work did not get any financial support from any organisation.

CRediT authorship contribution statement

G. Venkatesh: Conceptualization, Writing – original draft. **S. Haseena:** Supervision. **P. Vennila:** Visualization. **Yudibeth Sixto-López:** Formal analysis. **V. Siva:** Methodology. **J.N. Cheerlin Mishma:** Conceptualization. **S. Abul Kalam Azad:** Data curation. **Y. Sheena Mary:** Resources.

Declaration of competing interest

The authors declare that they have no known competing financial interests or personal relationships that could have appeared to influence the work reported in this paper.

Data availability

No data was used for the research described in the article.

Supplementary materials

Supplementary material associated with this article can be found, in the online version, at doi:10.1016/j.chphi.2024.100481.

References

[1] R.C. Mohs, N.H. Greig, Drug discovery and development: role of basic biological research, Alzheimers Dement (N Y) 11 (2017) 651–657, https://doi.org/10.1016/j.trci.2017.10.005.
[2] K.C. Nicolaou, The chemistry-biology-medicine continuum and the drug discovery and development process in academia, Chem. Biol. 21 (2014) 1039–1045, https://doi.org/10.1016/j.chembiol.2014.07.020.
[3] K.C. Nicolaou, The emergence of the structure of the molecule and the art of its synthesis, Angew. Chem. 52 (2013) 131–146.
[4] K. Makrilakis, The role of DPP-4 inhibitors in the treatment algorithm of type 2 diabetes mellitus: when to select, what to expect, Int. J. Environ. Res. Public Health 16 (2019) 2720, https://doi.org/10.3390/ijerph16152720.
[5] S. Padhi, A. Kumar Nayak, A. Behera, Type II diabetes mellitus: a review on recent drug based therapeutics, Biomed. Pharmacother. 131 (2020) 110708, https://doi.org/10.1016/j.biopha.2020.110708.

[6] S. Hædersdal, A. Lund, FK. Knop, T. Vilsbøll, The role of glucagon in the pathophysiology and treatment of type 2 diabetes, Mayo Clin. Proc. 93 (2018) 217–239, https://doi.org/10.1016/j.mayocp.2017.12.003.

[7] R.M. Lu, Y.C. Hwang, I.J. Liu, C.C. Lee, H.Z. Tsai, H.J. Li, H.C. Wu, Development of therapeutic antibodies for the treatment of diseases, J. Biomed. Sci. 27 (2020) 1, https://doi.org/10.1186/s12929-019-0592-z.

[8] J. Green, M. Feinglos, New combination treatments in the management of diabetes: focus on sitagliptin-metformin, Vasc. Health Risk Manag. 4 (2008) 743–751, https://doi.org/10.2147/vhrm.s3105.

[9] S.A. Miller, E.L. St Onge, J.R. Accardi, Sitagliptin as combination therapy in the treatment of type 2 diabetes mellitus, Diabetes Metab. Syndr. Obes. 13 (2009) 23–30, https://doi.org/10.2147/dmsott.s4068.

[10] S. Alam, M.K. Hasan, S. Neaz, N. Hussain, M.F. Hossain, T. Rahman, Diabetes mellitus: insights from epidemiology, biochemistry, risk factors, diagnosis, complications and comprehensive management, Diabetology 2 (2021) 36–50, https://doi.org/10.3390/diabetology2020004.

[11] D. Röhrborn, N. Wronkowitz, J. Eckel, DPP4 in diabetes, Front.Immunol. 27 (2015) 386, https://doi.org/10.3389/fimmu.2015.00386.

[12] R. Godinho, C. Mega, E. Teixeira-de-Lemos, E. Carvalho, F. Teixeira, R. Fernandes, F. Reis, The place of dipeptidyl peptidase-4 inhibitors in type 2 diabetes therapeutics: a "Me too" or "The special one" antidiabetic class? J. Diabetes. Res. 9 (2015) 806979 https://doi.org/10.1155/2015/806979.

[13] T.D. Müller, B. Finan, S.R. Bloom, D. D'Alessio, D.J. Drucker, P.R. Flatt, A. Fritsche, F. Gribble, H.J. Grill, J.F Habener, J.J. Holst, W. Langhans, J.J. Meier, M.A. Nauck, D. Perez-Tilve, A. Pocai, F. Reimann, D.A. Sandoval, T.W. Schwartz, R.J. Seeley, K. Stemmer, M. Tang-Christensen, S.C. Woods, R.D. DiMarchi, M.H. Tschöp, Glucagon-like peptide 1 (GLP-1), Mol. Metab. 30 (2019) 72–130, https://doi.org/10.1016/j.molmet.2019.09.010.

[14] E.L. St Onge, S. Miller, E. Clements, Sitagliptin/Metformin (janumet) as combination therapy in the treatment of type-2 diabetes mellitus, Pharm. Therap. 37 (2012) 699–708. PMID: 23319848.

[15] M. Sakamoto, R. Nishimura, T. Irako, D. Tsujino, K. Ando, K. Utsunomiya, Comparison of vildagliptin twice daily vs. sitagliptin once daily using continuous glucose monitoring (CGM): crossover pilot study (J-VICTORIA study), Cardiovasc. Diabetol. 11 (2012) 92, https://doi.org/10.1186/1475-2840-11-92.

[16] A. Gumieniczek, A. Berecka, T. Mroczek, K. Wojtanowski, K. Dąbrowska, K. Stępień, Determination of chemical stability of sitagliptin by LC-UV, LC-MS and FT-IR methods, J. Pharm. Biomed. Anal. 164 (7) (2019) 89–807, https://doi.org/10.1016/j.jpba.2018.11.023.

[17] M. Medimagh, N. Issaoui, S. Gatfaoui, O. Al-Dossary, AS. Kazachenko, H. Marouani, M.J. Wojcik, Molecular modeling and biological activity analysis of new organic-inorganic hybrid: 2-(3,4-dihydroxyphenyl) ethanaminium nitrate, J. King Saud Univ. Sci 33 (2021) 101616, https://doi.org/10.1016/j.jksus.2021.101616.

[18] A. Jumabaev, U. Holikulov, H. Hushvaktov, I. Noureddine, A. Absanov, Intermolecular interactions in ethanol solution of OABA: Raman, FT-IR, DFT, M062X, MEP, NBO, FMO, AIM, NCI, RDG analysis, J. Mol. Liq. 377 (2023) 121552, https://doi.org/10.1016/j.molliq.2023.121552.

[19] O. Noureddine, N. Issaoui, S. Gatfaoui, O. Al-Dossary, H. Marouani, Quantum chemical calculations, spectroscopic properties and molecular docking studies of a novel piperazine derivative, J. King Saud Univ. Sci. 33 (2021) 101283, https://doi.org/10.1016/j.jksus.2020.101283.

[20] A.S. Kazachenko, Y.N. Malyar, N.Y. Vasilyeva, V.S. Borovkova, N. Issaoui, Optimization of guar gum galactomannan sulfation process with sulfamic acid, Biomass Conv. Bioref. 13 (2023) 10041–10050, https://doi.org/10.1007/s13399-021-01895-y.

[21] JS. Al-Otaibi, Y.S Mary, Y. Shyma Mary, A. Mondal, N. Acharjee, J. Gawad, Insights on adsorption properties of a DNA base, guanine on nano metal cages (Ag24/Au24/Cu24): DFT, SERS, NCI and solvent effects, J. Mol. Struct. 1285 (2023) 135541, https://doi.org/10.1016/j.molstruc.2023.135541.

[22] Y.S Mary, Y.S Mary, M. Krátký, J. Vinsova, J. Gawad, M.C. Gamberini, The concentration dependent SERS studies of a bioactive 4-chlorobenzylidene derivative: experimental and DFT investigations, J. Mol. Liq. 381 (2023) 121855, https://doi.org/10.1016/j.molliq.2023.121855.

[23] JS. Al-Otaibi, Y.S Mary, Y. Shyma Mary, M. Krátký, J. Vinsova, M.C. Gamberini, Concentration dependent SERS profile of p-tolyl 2-acetamido-3-(4-fluorophenyl) propanoate (AFP) in silver colloidal nanohydrosols: experimental and DFT investigations, J. Mol. Struct. 1290 (2023) 135998, https://doi.org/10.1016/j.molstruc.2023.135998.

[24] G. Raja, G. Venkatesh, JS. Al-Otaibi, P. Vennila, Y. Sheena Mary, Y. Sixto-López, Synthesis, characterization, molecular docking and molecular dynamics simulations of benzamide derivatives as potential anti-ovarian cancer agents, J. Mol. Struct. 1269 (2022) 133785.

[25] JS. Al-Otaibi, Y.S Mary, Y. Shyma Mary, R. Thomas, Evidence of cluster formation of pyrrole with mixed silver metal clusters, Agx-My (x = 4,5, y = 2/1 and M = Au/Ni/Cu) using DFT/SERS analysis, Comput. Theor. Chem. 1208 (2022) 113569, https://doi.org/10.1016/j.comptc.2021.113569.

[26] A. Monpezat, J. Aupiais, B. Siberchicot, Xe adsorption on noble metal clusters: a density functional theory investigation, ACS Omega 47 (2021) 31513–31519, https://doi.org/10.1021/acsomega.1c03849.

[27] G. Venkatesh, Y. Sixto-López, P. Vennila, Y. Sheena Mary, J. Correa-Basurto, Y. Shyma Mary, A. Manikandan, An investigation on the molecular structure, interaction with metal clusters, anti-Covid-19 ability of 2-deoxy-D-glucose: DFT calculations, MD and docking simulations, J. Mol. Struct. 1258 (2022) 132678.

[28] JS. Al-Otaibi, Y.S Mary, Y. Shyma Mary, R. Trivedi, B. Chakrabory, R. Thomas, Cluster formation between an oxadiazole derivative with metal nanoclusters (Ag/Au/Cu), graphene quantum dot sheets, SERS studies, and solvent effects, Struct. Chem. 34 (2023) 867–877.

[29] JS. Al-Otaibi, Y.S Mary, Y. Shyma Mary, R. Thomas, Renyer Alves Costa, DFT investigations on the interactions between pyrimidine derivatives and Ag/Au/Cu metal clusters: solvation effects and reactivity analysis, J. Clust. Sci. (2023), https://doi.org/10.1007/s10876-023-02429-4.

[30] S. Divya, P. Sivaprakash, S. Raja, S. Esakki Muthu, I. Kim, N. Renuka, S. Arumugam, T.H. Oh, Impact of Zn doping on the dielectric and magnetic properties of $CoFe_2O_4$ nanoparticles, Ceram. Int. 48 (2022) 33208–33218.

[31] G. Venkatesh, S. Haseena, JS. Al-Otaibi, Y. Sheena Mary, P. Vennila, Y. Shyma Mary, S. AbulKalam Azad, Observations into the reactivity, docking, DFT, and MD simulations of fludarabine and clofarabine in various solvents, J. Mol. Liq. 383 (2023) 122076, https://doi.org/10.1016/j.molliq.2023.122076.

[32] K. Periyasamy, P. Sakthivel, P. Vennila, P.M. Anbarasan, G. Venkatesh, Y.S Mary, Novel D-π-A phenothiazine and dibenzofuran organic dyes with simple structures for efficient dye-sensitized solar cells, J. Photochem. Photobiol. A 413 (2021) 113269, https://doi.org/10.1016/j.jphotochem.2021.113269.

[33] N. Ye, Z. Yang, Y. Liu, Applications of density functional theory in COVID-19 drug modeling, Drug Discov. Today 27 (2022) 1411–1419, https://doi.org/10.1016/j.drudis.2021.12.017.

[34] P. Vennila, JS. Al-Otaibi, G. Venkatesh, Y. Sheena Mary, V. Raj, N. Acharje, P. Tamilselvi, Structural, spectral, molecular docking, and molecular dynamics simulations of phenylthiophene-2-carboxylate compounds as potential anticancer agents, Polycycl. Aromat. Compd. (2023), https://doi.org/10.1080/10406638.2023.2172052.

[35] P. Surendar, T. Pooventhiran, N. Al-Zaqri, S. Rajam, D. Jagadeeswara Rao, R. Thomas, Synthesis of three quasi liquid Schiff bases between hexanal and adenine, cytosine, and l-leucine, structural interpretation, quantum mechanical studies and biological activity prediction, J. Mol. Liq. 341 (2021) 117305, https://doi.org/10.1016/j.molliq.2021.117305.

[36] J. Geethapriya, A. Shanthidevi, M. Arivazhagan, N. Elangovan, R. Thomas, Synthesis, structural, DFT, quantum chemical modeling and molecular docking studies of (E)-4-(((5-methylfuran-2-yl)methylene)amino) benzenesulfonamide from 5-methyl-2-furaldehyde and sulfanilamide, J. Indian Chem. Soc. 99 (2022) 100418, https://doi.org/10.1016/j.jics.2022.100418.

[37] AM. John, J. Jose, R. Thomas, KJ. Thomas, SP. Balakrishnan, Spectroscopic and TDDFT investigation of highly selective fluoride sensors by substituted acyl hydrazones, Spectrochim. Acta Part A Mol. Biomol. Spectrosc. 236 (2020) 118329, https://doi.org/10.1016/j.saa.2020.118329.

[38] P.R. Kavitha Rani, Y. Sheena Mary, A. Fernandez, A.P. S, Y. Shyma Mary, R. Thomas, Single crystal XRD, DFT investigations and molecular docking study of 2- ((1,5-dimethyl-3-oxo-2-phenyl-2,3-dihydro-1H-pyrazol-4-yl)amino) naphthalene-1,4-dione as a potential anti- cancer lead molecule, Comput. Biol. Chem. 78 (2019) 153–164, https://doi.org/10.1016/j.compbiolchem.2018.11.022.

[39] OA.A Ali, N. Elangovan, SF. Mahmoud, MS. El-Gendey, H.Z.E. Elbasheer, SM. El-Bahy, R. Thomas, Synthesis, characterization, vibrational analysis and computational studies of a new Schiff base from pentafluoro benzaldehyde and sulfanilamide, J. Mol. Struct. 1265 (2022) 133445, https://doi.org/10.1016/j.molstruc.2022.133445.

[40] S. Sowrirajan, N. Elangovan, G. Ajithkumar, A. Sirajunnisa, B.R. Venkatraman, MM. Ibrahim, GA.M. Mersal, Renjith Thomas, Synthesis, spectral, structural features, electronic properties, biological activities, computational, wave function properties, and molecular docking studies of (E)-4-(((pentafluorophenyl) methylene) amino)-N-(pyrimidin2-yl)benzenesulfonamide, J. Mol. Struct. 1265 (2022) 133472, https://doi.org/10.1016/j.molstruc.2022.133472.

[41] M.J. Frisch, G.W. Trucks, H.B. Schlegel, G.E. Scuseria, M.A. Robb, J.R. Cheeseman, J.A. Montgomery Jr., T. Vreven, K.N. Kudin, J.C. Burant, J.M. Millam, S.S. Iyengar, J. Tomasi, V. Barone, B. Mennucci, M. Cossi, G. Scalmani, N. Rega, G. A. Petersson, H. Nakatsuji, M. Hada, M. Ehara, K. Toyota, R. Fukuda, J. Asegawa, M. Ishida, T. Nakajima, Y. Honda, O. Kitao, H. Nakai, M. Klene, X. Li, J. E. Knox, H. P. Hratchian, J. B. Cross, C. Adamo, J. Jaramillo, R. Gomperts, R. E. Stratmann, O. Yazyev, A. J. Austin, R. Cammi, C. Pomelli, J. W. Ochterski, P. Y. Ayala, K. Morokuma, G. A. Voth, P. Salvador, J. J. Dannenberg, V. G. Zakrzewski, S. Dapprich, A. D. Daniels, M. C. Strain, O. Farkas, D. K. Malick, A. D. Rabuck, K. Raghavachari, J. B. Foresman, J. V. Ortiz, Q. Cui, A. G. Baboul, S. Clifford, J. Ioslowski, B. B. Stefanov, G. Liu, A. Liashenko, P. Piskorz, I. Komaromi, R. L. Martin, D. J. Fox, T. Keith, M. A. AlLaham, C. Y. Peng, A. Nanayakkara, M. Challacombe, P. M. W. Gill, B. Johnson, W. Chen, M. W. Wong, C. Gonzalez, J. A. Pople, Gaussian 03, Revision E. 01, 121, Gaussian Inc,. Pittsburgh. B. A. 2000, Walliford CT, 2009, p. 150.

[42] M.H. Jamroz, Vibrational Energy Distribution Analysis VEDA 4, Warsaw, 2004.

[43] A.D. Isravel, J.K. Jeyaraj, S. Thangasamy, W.J. John, DFT, NBO, HOMO-LUMO, NCI, stability, Fukui function and hole–Electron analyses of tolcapone, Comput. Theor. Chem. 1202 (2021) 113296.

[44] S.R. Lin, C.H. Chang, M.J. Tsai, H. Cheng, J.C. Chen, M.K. Leong, C.F. Weng, The perceptions of natural compounds against dipeptidyl peptidase 4 in diabetes: from in silico to in vivo, Therap. Adv. Chronic Dis. (2019) 10, https://doi.org/10.1177/2040622319875305.

[45] BIOVIA, Dassault Systèmes, Discovery Studio, version 17 R2, Dassault Systèmes, San Diego, 2017.

[46] D. van der Spoel, E. Lindahl, B. Hess, G. Groenhof, A.E. Mark, H.J.C. Berendsen, GROMACS: fast, flexible and free, J. Comp. Chem. 26 (2023) 1701–1718, https://doi.org/10.1002/jcc.20291 (2005).

[47] M. Bugnon, M. Goullieux, U.F. Röhrig, M.A.S. Perez, A. Daina, O. Michielin, V. Zoete, S. Param, A modern web-based tool for efficient small molecule

parametrization, J. Chem. Inf. Model. (2023), https://doi.org/10.1021/acs.jcim.3c01053 (2023).
[48] V. MarvinSketch, 22. 13. 0, calculation module developed by ChemAxon, http://www.chemaxon.com/products/marvin/marvinsketch/, (2022).
[49] T. Darden, D. York, L. Pedersen, Particle mesh Ewald: An N·log(N) method for Ewald sums in large systems, J. Chem. Phys. 98 (1993) 10089–10092, https://doi.org/10.1063/1.464397.
[50] G. Malloci, G. Serra, A. Bosin, A. Vargiu, Extracting conformational ensembles of small molecules from molecular dynamics simulations: ampicillin as a test case, Computation 4 (2016) 5, https://doi.org/10.3390/computation4010005.
[51] P. Vennila, G. Venkatesh, Y. Sixto-López, C. Kamal, S. Kaya, G. Serdaroğlu, B. Landeros-Rivera, Synthesis, spectroscopic characterization, molecular docking studies and DFT calculation of novel Mannich base 1-((4-ethylpiperazin-1-yl)(2-hydroxyphenyl)methyl)naphthalen-2-ol, J. Mol. Struct. 1246 (2021) 131164, https://doi.org/10.1016/j.molstruc.2021.131164.
[52] AS. Kazachenko, M. Medimagh, N. Issaoui, O. Al-Dossary, MJ. Wojcik, AS. Kazachenko, AV. Miroshnokova, YN. Malyar, Sulfamic acid/water complexes (SAA-H2O(1-8)) intermolecular hydrogen bond interactions: FTIR,X-ray, DFT and AIM analysis, J. Mol. Struct. 1265 (2022) 133394, https://doi.org/10.1016/j.molstruc.2022.133394.
[53] S. Gatfaoui, N. Issaoui, T. Roisnel, Houda Marouani, Synthesis, experimental and computational study of a non-centrosymmetric material 3-methylbenzylammonium trioxonitrate, J. Mol. Struct. 1225 (2021) 129132, https://doi.org/10.1016/j.molstruc.2020.129132.
[54] K. Vanasundari, V. Balachandran, M. Kavimani, B. Narayana, Spectroscopic investigation, vibrational assignments, Fukui functions, HOMO-LUMO, MEP and molecular docking evaluation of 4 – [(3, 4 – dichlorophenyl) amino] 2 – methylidene 4 – oxo butanoic acid by DFT method, J. Mol. Struct. 1147 (2017) 136–147, https://doi.org/10.1016/j.molstruc.2017.06.096.
[55] N.C.F. Stofella, A. Veiga, L.J. Oliveira, E.F. Montin EF, M.A.S.C.F. Andreazza, L. S. Bernardi, P.R. Oliveira, F.S. Murakami, Solid-state characterization of different crystalline forms of Sitagliptin, Materials 12 (2019) 2351, https://doi.org/10.3390/ma12152351.
[56] S. Rajesh, S. Gunasekaran, P. Rajesh, HOMO-LUMO, NBO and vibrational analysis of Sitagliptin by using DFT calculations and experimental study (FT-IR, FT-Raman and UV-Visible Spectroscopies), Int. J. ChemTech Res. 11 (2018) 107–122.
[57] T. Saravana Kumaran, A. Prakasam, P.M. Anbarasan, P. Vennila, G. Venkatesh, S. Parveen Banu, Y. Sheena Mary, New phenoxazine-based organic dyes with various acceptors for dye-sensitized solar cells: synthesis, characterization, DSSCs fbrications and DFT study, J. Comput. Biophys. Chem. 20 (2021) 465–476, https://doi.org/10.1142/S2737416521500253.
[58] T. Saravana Kumaran, A. Prakasam, G. Venkatesh, P. Vennila, Y. Sheena Mary, S. Parveen Banu, Design and synthesis of phenylacridine-based on organic dyes and its applications in dye-sensitized solar cells, Russ. J. Phys. Chem. A 97 (2023) 2607–2623, https://doi.org/10.1134/S0036024423110298.
[59] K. Periyasamy, P. Sakthivel, G. Venkatesh, P. Vennila, Y.S Mary, Synthesis and design of carbazole-based organic sensitizers for DSSCs applications: experimental and theoretical approaches, Chem. Pap. (2023), https://doi.org/10.1007/s11696-023-03101-x.
[60] K. Periyasamy, P. Sakthivel, G. Venkatesh, P. Vennila, Y. Sheena Mary, S. Haseena, Structural and photophysical studies of triphenylamine-based organic dyes for applications in DSSCs: experimental and DFT analysis, Polycycl. Aromat. Compd. (2023), https://doi.org/10.1080/10406638.2023.2264450.
[61] H.K. Pathan, G. Khanum, R. Javed, N. Siddiqui, S. Selvakumari, S. Muthu, A. Ali, H. Arora, M. Afzal, A. Kumar, S. Javed, Quantum computational, spectroscopic characterization, Hirshfeld analysis & molecular docking studies on p-toluenesulfonic acid (p-TSA) or tosylic acid, Chem. Phys. Impact 7 (2023) 100320.
[62] T. Pooventhiran, A.Y. Abdullah Alzahrani, K.J. Rajimon, R. Thomas, Solvent interaction and dynamics of neurotransmitters l-aspartic acid and l-glutamic acid with water and ethanol, J. Mol. Struct. 1273 (2023) 134347.
[63] T. Saravanakumaran, A. Prakasam, G. Venkatesh, C. Kamal, Y. Sheena Mary, S. Parveen Banu, P. Vennila, Y. Shyma Mary, Synthesis, spectral characterizations, molecular geometries and electronic properties of phenothiazine based organic dyes for dye-sensitized solar cells, Z. Phys. Chem. 235 (2021) 1355–1380, https://doi.org/10.1515/zpch-2020-1732.
[64] P. Vennila, M. Govindaraju, G. Venkatesh, C. Kamal, Molecular structure, vibrational spectral assignments (FT-IR and FT-RAMAN), NMR, NBO, HOMO-LUMO and NLO properties of O-methoxybenzaldehyde based on DFT calculations, J. Mol. Struct. 1111 (2016) 151–156, https://doi.org/10.1016/j.molstruc.2016.01.068.
[65] B. Chettri, P.K. Patra, S. Verma, B.K. Rao, M.L. Verma, V. Thakur, D.P. Rai, Induced magnetic states upon electron–hole injection at B and N sites of hexagonal boron nitride bilayer: A density functional theory study, Int. J. Quantum Chem. 121 (2021) 26680.
[66] E.R. Johnson, S. Keinan, P. Mori-Sánchez, J. Contreras-García, A.J. Cohen, W. Yang, Revealing noncovalent interactions, J. Am. Chem. Soc. 132 (2010) 6498–6506.
[67] AS. Kazachenko, M. Medimagh, N. Issaoui, O. Al-Dossary, MJ. Wojcik, AS. Kazachenko, AV. Miroshnokova, YN. Malyar, Sulfamic acid/water complexes (SAA-H2O(1-8)) intermolecular hydrogen bond interactions: FT-IR,X-ray, DFT and AIM analysis, J. Mol. Struct. 1265 (2022) 133394, https://doi.org/10.1016/j.molstruc.2022.133394.
[68] C. Daghar, N. Issaoui, T. Roisnel, V. Dorcet, H. Marouani, Empirical and computational studies on newly synthesis cyclohexylammonium perchlorate, J. Mol. Struct. 1230 (2021) 129820, https://doi.org/10.1016/j.molstruc.2020.129820.
[69] A. Jumabaev, U. Holikulov, H. Hushvaktov, I. Noureddine, A. Absanov, Intermolecular interactions in ethanol solution of OABA: Raman, FTIR, DFT, M062X, MEP, NBO, FMO, AIM, NCI, RDG analysis, J. Mol. Liq. 377 (2023) 121552, https://doi.org/10.1016/j.molliq.2023.121552.
[70] S. Shukla, A. Srivastava, P. Kumar, P. Tandon, R. Maurya, R.B. Singh, Vibrational spectroscopic, NBO, AIM, and multiwfn study of tectorigenin: a DFT approach, J. Mol. Struct. 1217 (2020) 128443, https://doi.org/10.1016/j.molstruc.2020.128443.
[71] J.C. Mishma, V.B. Jothy, A. Irfan, B. Narayana, S.N. Kodlady, S. Muthu, Solvent potential effects (topological aspects, electron excitation), spectral characterization and biological attributes of NLO active 1-(2, 4-dinitrophenyl)-2-((E)-3-phenylallylidene) hydrazine: multiple anti tuberculosis agent, J. Mol. Liq. 376 (2023) 121439.
[72] S. Janani, H. Rajagopal, S. Muthu, S. Aayisha, M. Raja, Molecular structure, spectroscopic (FT-IR, FT-Raman, NMR), HOMO-LUMO, chemical reactivity, AIM, ELF, LOL and Molecular docking studies on 1-Benzyl-4-(N-Boc-amino) piperidine, J. Mol. Struct. 1230 (2021) 129657.
[73] S. Sevvanthi, S. Muthu, S. Aayisha, P. Ramesh, M. Raja, Spectroscopic (FT-IR, FT-Raman and UV-Vis), computational (ELF, LOL, NBO, HOMO-LUMO, Fukui, MEP) studies and molecular docking on benzodiazepine derivatives-heterocyclic organic arenes, Chem. Data Collect. 30 (2020) 100574.
[74] S. Khan, H. Sajid, K. Ayub, T. Mahmood, Adsorption behaviour of chronic blistering agents on graphdiyne; excellent correlation among SAPT, reduced density gradient (RDG) and QTAIM analyses, J. Mol. Liq. 316 (2020) 113860, https://doi.org/10.1016/j.molliq.2020.113860.